ÖAW AUSTRIAN ACADEMY OF SCIENCES

RICAM – JOHANN RADON INSTITUTE FOR COMPUTATIONAL AND APPLIED MATHEMATICS

Inversion of the Momenta Doppler Transform in two dimensions

H. Fujiwara, D. Omogbhe, K. Sadiq, A. Tamasan

RICAM-Report 2023-20

INVERSION OF THE MOMENTA DOPPLER TRANSFORM IN TWO DIMENSIONS

HIROSHI FUJIWARA, DAVID OMOGBHE, KAMRAN SADIQ, AND ALEXANDRU TAMASAN

ABSTRACT. We introduce an analytic method which stably reconstructs both components of a (sufficiently) smooth, real valued, vector field compactly supported in the plane from knowledge of its Doppler transform and its first moment Doppler transform. The method of proof is constructive. Numerical inversion results indicate robustness of the method.

1. INTRODUCTION

We revisit the problem of inversion of the Doppler transform

$$D^0\mathbf{F}(x,\boldsymbol{\theta}) := \int_{-\infty}^{\infty} \boldsymbol{\theta}\cdot\mathbf{F}(x+t\boldsymbol{\theta})dt, \quad (x,\boldsymbol{\theta})\in\mathbb{R}^2\times\mathbf{S}^1, \tag{1}$$

of a real valued vector field $\mathbf{F}$ compactly supported in the plane. It is easy to note that D^0 has a large kernel containing all the gradient fields vanishing at the boundary of the support. In response, a vast literature in tensor tomography concerns recovery questions (uniqueness, stability, reconstruction) on the solenoidal part of the tensor field; see the surveys [23, 17, 8, 4, 16, 22] and reference therein. The problem is originally motivated by engineering practices [29, 14, 2, 24].

In this paper, we consider the inversion problem introduced (for arbitrary order tensors) in [23]. In particular for 1-order tensors: $\mathbf{F}$ is to be determined from $D^0\mathbf{F}$ and its first-moment-Doppler transform:

$$D^1\mathbf{F}(x,\boldsymbol{\theta}) := \int_{-\infty}^{\infty} t\boldsymbol{\theta}\cdot\mathbf{F}(\Pi_{\boldsymbol{\theta}}(x)+t\boldsymbol{\theta})dt, \quad (x,\boldsymbol{\theta})\in\mathbb{R}^2\times\mathbf{S}^1, \tag{2}$$

where $\Pi_{\boldsymbol{\theta}}(x) = x-(x\cdot\boldsymbol{\theta})\boldsymbol{\theta}$ is the projection of x onto $\boldsymbol{\theta}^\perp$.

Note that the first momentum transform $I^1\mathbf{F}$ in [23] is defined on the unit tangent bundle of the domain, while $D^1\mathbf{F}$ here is normalized to the tangent bundle of the circle. However, there is an one-to-one correspondence between $D^1\mathbf{F}$ and $I^1\mathbf{F}$ (affine in $x\cdot\boldsymbol{\theta}$ with coefficients dependent on $(x\cdot\boldsymbol{\theta}^\perp,\boldsymbol{\theta})$). Modulo this correspondence, the unique determination of the full vector field $\mathbf{F}$ from $(D^0\mathbf{F}, D^1\mathbf{F})$ has been shown in [23, 13], while stability estimates and inversions are proposed in [10, 11], and most recently in [12]. The latter work also includes a numerical implementation.

Different from the above referenced works, in here we introduce a new reconstruction method of the full vector field (see the proof of Theorem 1.1), which is based on Bukhgeim's theory of A-analyticity [3] and its extension in [18, 21, 20]. Numerical results from its implementation are also presented. Specific to two dimensions, the method solves an inverse boundary value problem for a coupled system of Bukhgeim-Beltrami equations. Used in the stability estimates, but of independent interest, we establish a priori estimates for higher order derivatives of solutions of the inhomogenous Bukhgeim-Beltrami equation; see Theorem 2.2.

Date: July 20, 2023.

2010 *Mathematics Subject Classification.* Primary 35J56, 30E20; Secondary 35R30, 45E05.

Key words and phrases. Doppler tomography, momentum transform, full vector field reconstruction, stability estimate, A-analytic maps, Bukhgeim-Beltrami equation, vector tomography.

We mention that Bukhgeim's approach has also been used in the determination of the attenuated X-ray transform of compactly supported functions in the plane [1], of the solenoidal part of a vector field $\mathbf{F}$ from its Doppler transform in [9, 26, 15]. The full vector field has been recovered from the weighted Doppler transform, with a weight arising from a positive attenuation factor [27, 26, 19]. We stress that our problem here is different, since it corresponds to the zero attenuation case.

Throughout, $\mathbf{F}$ is a real valued vector field with support contained in a disc Ω of some *known* large enough radius. We also assume $\mathbf{F} \in H_0^2(\Omega;\mathbb{R}^2)$. Upon a translation and scaling, without loss of generality, $\mathbf{F}$ is supported in the unit disc $\Omega = \{z \in \mathbb{C} : |z| < 1\}$. The boundary Γ of Ω is the unit circle, but we keep this notation to differentiate from the set $\mathbf{S}^1$ of directions.

Functions u on $\Omega \times \mathbf{S}^1$ are characterized by the sequence valued map of their Fourier coefficients $u_{-n}(z) = \frac{1}{2\pi}\int_0^{2\pi} u(z,\boldsymbol{\theta})e^{in\theta}d\theta$ (non-positive indexes are sufficient) in the angular variable,

$$\Omega \ni z \mapsto \mathbf{u}(z) := \langle u_0(z), u_{-1}(z), u_{-2}(z), \cdots\rangle.$$

We work in the spaces

$$l^{2,p}(\mathbb{N}; H^q(\Omega)) := \left\{ \mathbf{u} = \langle u_0, u_{-1}, u_{-2}, \cdots\rangle : \|\mathbf{u}\|_{p,q}^2 := \sum_{j=0}^{\infty}(1+j)^{2p}\left\|u_{-j}\right\|_{H^q(\Omega)}^2 < \infty \right\}. \tag{3}$$

The first index p encodes the smoothness of u in the angular variable, while the second index q shows the smoothness in the spatial variable. The traces $\mathbf{g} = \mathbf{u}|_\Gamma$ on Γ of maps $\mathbf{u} \in l^{2,p}(\mathbb{N}; H^q(\Omega))$ are in $l^{2,p}(\mathbb{N}; H^{q-\frac{1}{2}}(\Gamma))$ endowed with the norm

$$\|\mathbf{g}\|_{p,q-\frac{1}{2}}^2 := \sum_{j=0}^{\infty}(1+j)^{2p}\left\|g_{-j}\right\|_{H^{q-\frac{1}{2}}(\Gamma)}^2. \tag{4}$$

Furthermore, since Γ is the unit circle, the $H^{q-\frac{1}{2}}(\Gamma)$-norm of g_{-j} are defined in the Fourier domain by

$$\left\|g_{-j}\right\|_{H^{q-\frac{1}{2}}(\Gamma)}^2 = \sum_{k=-\infty}^{\infty}(1+|k|)^{2q-1}|g_{-j,k}|^2, \tag{5}$$

where $g_{-j,k} = \dfrac{1}{2\pi}\displaystyle\int_0^{2\pi} g_{-j}(e^{i\beta})e^{-ik\beta}d\beta$, for $k \in \mathbb{Z}$, $j \geqslant 0$. In particular, for $\mathbf{g} \in l^{2,p}(\mathbb{N}; H^{q-\frac{1}{2}}(\Gamma))$,

$$\|\mathbf{g}\|_{p,q-\frac{1}{2}}^2 = \sum_{j=0}^{\infty}\sum_{n=-\infty}^{\infty}(1+j)^{2p}(1+|n|)^{2q-1}|g_{-j,n}|^2. \tag{6}$$

Note that both $D^0\mathbf{F}$ and $D^1\mathbf{F}$ are functions on the lines, which vanish on lines laying outside Ω. Upon parametrizing the lines intersecting Ω by points on the torus $\Gamma \times \mathbf{S}^1$, $D^0\mathbf{F}$ and $D^1\mathbf{F}$ are understood as functions on the torus; see Figure 1 for an example.

For brevity we adopt throughout the notation $\|\mathbf{v}\| \lesssim \|\mathbf{w}\|$, whenever $\|\mathbf{v}\| \leqslant C\|\mathbf{w}\|$ for some constant $C > 0$ independent of $\mathbf{v}$ and $\mathbf{w}$.

Theorem 1.1. *Let $\Omega \subset \mathbb{R}^2$ be the unit disc and $\mathbf{F} = \langle F_1, F_2\rangle$ be some unknown real valued vector field compactly supported in Ω. If $\mathbf{F} \in H_0^2(\Omega;\mathbb{R}^2)$, then*

$$D^0\mathbf{F}, D^1\mathbf{F} \in H^{\frac{3}{2}}(\mathbf{S}^1; H^{\frac{3}{2}}(\Gamma)), \tag{7}$$

and $\mathbf{F}$ is uniquely determined by $D^0\mathbf{F}$ and $D^1\mathbf{F}$ with the estimate

$$\|\mathbf{F}\|_{L^2(\Omega)}^2 \lesssim \left\|D^0\mathbf{F}\right\|_{\frac{3}{2},\frac{1}{2}}^2 + \left\|D^1\mathbf{F}\right\|_{\frac{3}{2},\frac{3}{2}}^2. \tag{8}$$

The method of proof is constructive.

2. Refined a priori estimates for the inhomogenous Bukhgeim-Beltrami equation

The stability estimate in Theorem 1.1 requires a-priori estimates for higher order derivatives of solution of the inhomogenous Bukhgeim-Beltrami equation

$$\overline{\partial}\mathbf{v} + L^2\partial\mathbf{v} = \mathbf{w}, \tag{9}$$

where

$$L\mathbf{v} = L(v_0, v_{-1}, v_{-2}, \cdots) := (v_{-1}, v_{-2}, \cdots)$$

denotes the left translation, and

$$\overline{\partial} = \frac{1}{2}(\partial_{x_1} + i\partial_{x_2}), \quad \partial = \frac{1}{2}(\partial_{x_1} - i\partial_{x_2}) \tag{10}$$

are the Cauchy-Riemann operators.

Theorem 2.1. *Let* $\mathbf{w} \in l^{2,p+1}(\mathbb{N}; L^2(\Omega))$*, for some fixed* $p \geqslant 0$*. If* $\mathbf{v} \in l^{2,p+\frac{1}{2}}(\mathbb{N}; H^1(\Omega))$ *solves* (9)*, then*

$$\|\mathbf{v}\|^2_{p,1} \lesssim \|\mathbf{w}\|^2_{p+1,0} + \|\mathbf{v}|_\Gamma\|^2_{p+\frac{1}{2},\frac{1}{2}}\,. \tag{11}$$

Proof. We reason by induction in p. The case $p = 0$,

$$\|\mathbf{v}\|^2_{0,1} \lesssim \|\mathbf{w}\|^2_{1,0} + \|\mathbf{v}|_\Gamma\|^2_{\frac{1}{2},\frac{1}{2}}\,, \tag{12}$$

is established in [6, Corollary 4.1].

Assume next that (11) holds for p:

$$\|\mathbf{v}\|^2_{p,1} \lesssim \|\mathbf{w}\|^2_{p+1,0} + \|\mathbf{v}|_\Gamma\|^2_{p+\frac{1}{2},\frac{1}{2}}\,. \tag{13}$$

Since $\mathbf{v}$ solves (9), the left shifted sequence $L^n\mathbf{v}$ solves

$$\overline{\partial}L^n\mathbf{v} + L^2\partial L^n\mathbf{v} = L^n\mathbf{w}. \tag{14}$$

Using the estimate (13) for $L^n\mathbf{v}$ solutions of (14), and a summation over n, we get

$$\sum_{n=0}^{\infty}\|L^n\mathbf{v}\|^2_{p,1} \lesssim \sum_{n=0}^{\infty}\|L^n\mathbf{w}\|^2_{p+1,0} + \sum_{n=0}^{\infty}\|L^n\mathbf{v}|_\Gamma\|^2_{p+\frac{1}{2},\frac{1}{2}}\,, \tag{15}$$

provided the right-hand-side is finite.

By applying the Lemma A.1 (with $B = l^2(\mathbb{N}; H^q(\Omega))$ for $q = 1$, $q = 0$, and $q = \frac{1}{2}$), we obtain

$$\|\mathbf{v}\|^2_{p+\frac{1}{2},1} \lesssim \|\mathbf{w}\|^2_{p+\frac{3}{2},0} + \|\mathbf{v}|_\Gamma\|^2_{p+1,\frac{1}{2}}\,. \tag{16}$$

By using the estimate (16), for the sequence $L^m\mathbf{v}$ replacing $\mathbf{v}$ and $L^m\mathbf{w}$ replacing $\mathbf{w}$, a summation over m, and another application of Lemma A.1 (with $B = l^2(\mathbb{N}; H^q(\Omega))$ for $q = 1$, $q = 0$, and $q = \frac{1}{2}$), yields

$$\|\mathbf{v}\|^2_{p+1,1} \lesssim \|\mathbf{w}\|^2_{p+2,0} + \|\mathbf{v}|_\Gamma\|^2_{p+\frac{3}{2},\frac{1}{2}}\,. \tag{17}$$

Note that, by hypothesis, the right-hand-side is finite.

□

Theorem 2.2. *Let* $\mathbf{w} \in l^{2,\frac{3}{2}}(\mathbb{N}; H^1(\Omega))$*. If* $\mathbf{v} \in l^{2,\frac{3}{2}}(\mathbb{N}; H^2(\Omega))$ *solves* (9) *then*

$$\|\partial_\nu\mathbf{v}|_\Gamma\|^2_{\frac{1}{2},\frac{1}{2}} \lesssim \|\mathbf{v}|_\Gamma\|^2_{\frac{3}{2},\frac{3}{2}} + \|\mathbf{w}|_\Gamma\|^2_{\frac{3}{2},\frac{1}{2}}\,, \quad \textit{and} \tag{18}$$

$$\|\mathbf{v}\|^2_{0,2} \lesssim \|\mathbf{w}\|^2_{1,1} + \|\mathbf{w}|_\Gamma\|^2_{\frac{3}{2},\frac{1}{2}} + \|\mathbf{v}|_\Gamma\|^2_{\frac{3}{2},\frac{3}{2}}\,. \tag{19}$$

In (18) ∂_ν *is the normal derivative at the boundary* Γ*.*

Proof. A change of coordinates at the boundary point $e^{i\eta} \in \Gamma$ rewrites ∂, $\overline{\partial}$ in (10) in terms of the tangential and normal derivatives ∂_τ, ∂_ν as $\partial = e^{-i\eta}(\partial_\nu - i\partial_\tau)/2$ respectively $\overline{\partial} = e^{i\eta}(\partial_\nu + i\partial_\tau)/2$..

If $\mathbf{v} \in l^{2,1}(\mathbb{N}; H^2(\Omega))$, then $\partial_\nu \mathbf{v}|_\Gamma \in l^{2,1}(\mathbb{N}; H^{\frac{1}{2}}(\Gamma))$ and the restriction of (9) to the boundary,

$$[e^{2i\eta} + L^2](\partial_\nu \mathbf{v}|_\Gamma) = -i[e^{2i\eta} - L^2](\partial_\tau \mathbf{v}|_\Gamma) + 2e^{i\eta}\mathbf{w}|_\Gamma$$

holds in $H^{1/2}(\Gamma)$. With $\mu = ie^{i\eta}$ we get

$$[\mu^2 - L^2](\partial_\nu \mathbf{v}|_\Gamma) = -i[\mu^2 + L^2](\partial_\tau \mathbf{v}|_\Gamma) + 2i\mu\mathbf{w}|_\Gamma. \tag{20}$$

While the unit circle is in the spectrum of the left translation $L : l^2 \mapsto l^2$, the resolvent $(\lambda - L^2)^{-1}$ extends continuously from $|\lambda| > 1$ to $|\lambda| = 1$ as a bounded operator from $l^{2,1}$ to l^2; see Lemma A.2 in the appendix.

An application of Lemma A.2 to (20) estimates the normal derivative of solutions of (9) in terms of their tangential derivative,

$$\|\partial_\nu \mathbf{v}|_\Gamma\|_{H^{1/2}(\Gamma;l^2)} \lesssim \|\partial_\tau \mathbf{v}|_\Gamma\|_{H^{1/2}(\Gamma;l^{2,1})} + \|\mathbf{w}|_\Gamma\|_{H^{1/2}(\Gamma;l^{2,1})}\,. \tag{21}$$

In terms of the Sobolev norms on the unit circle Γ in (3), the above estimate becomes

$$\|\partial_\nu \mathbf{v}|_\Gamma\|^2_{0,\frac{1}{2}} \lesssim \|\partial_\tau \mathbf{v}|_\Gamma\|^2_{1,\frac{1}{2}} + \|\mathbf{w}|_\Gamma\|^2_{1,\frac{1}{2}} \lesssim \|\mathbf{v}|_\Gamma\|^2_{1,\frac{3}{2}} + \|\mathbf{w}|_\Gamma\|^2_{1,\frac{1}{2}}\,. \tag{22}$$

For each $n \geqslant 0$, the shifted sequence $L^n\mathbf{v}$ solves the shifted inhomogeneous Bukhgeim-Beltrami equation (14) and, thus, it satisfies the estimate (22) with $\mathbf{v}$ replaced by $L^n\mathbf{v}$, and $\mathbf{w}$ replaced by $L^n\mathbf{w}$. A summation in n yields

$$\sum_{n=0}^{\infty} \|\partial_\nu L^n\mathbf{v}|_\Gamma\|^2_{0,\frac{1}{2}} \lesssim \sum_{n=0}^{\infty} \|L^n\mathbf{v}|_\Gamma\|^2_{1,\frac{3}{2}} + \sum_{n=0}^{\infty} \|L^n\mathbf{w}|_\Gamma\|^2_{1,\frac{1}{2}} \tag{23}$$

provided the right-hand-side is finite.

By applying the Lemma A.1 (with $B = l^2(\mathbb{N}; H^q(\Omega))$ for $q = \frac{1}{2}$ and $q = \frac{3}{2}$) in (23) yields

$$\|\partial_\nu \mathbf{v}|_\Gamma\|^2_{\frac{1}{2},\frac{1}{2}} \lesssim \|\mathbf{v}|_\Gamma\|^2_{\frac{3}{2},\frac{3}{2}} + \|\mathbf{w}|_\Gamma\|^2_{\frac{3}{2},\frac{1}{2}}\,. \tag{24}$$

Since $\mathbf{v} \in l^{2,\frac{3}{2}}(\mathbb{N}; H^2(\Omega))$ by hypothesis, the right hand of (24) is finite.

This ends the proof of the first estimate in (18).

For the estimate in (19), we differentiate the equation (9):

$$\overline{\partial}(\nabla \mathbf{v}) + L^2\partial(\nabla \mathbf{v}) = \nabla \mathbf{w}, \tag{25}$$

where ∇ stands for either $\overline{\partial}$ or ∂ and apply (12) for solutions $\nabla\mathbf{v}$ of (25) to obtain

$$\|\mathbf{v}\|^2_{0,2} \lesssim \|\mathbf{w}\|^2_{1,1} + \|\mathbf{v}|_\Gamma\|^2_{\frac{1}{2},\frac{3}{2}} + \|\partial_\nu \mathbf{v}|_\Gamma\|^2_{\frac{1}{2},\frac{1}{2}}\,. \tag{26}$$

An application of the estimate (18) to the last term in (26) concludes the proof of (19). □

3. Proof of Theorem 1.1

The reconstruction method is based on the equivalence with an inverse boundary value problem for a system of transport equations. We denote by $\Gamma_\pm := \{(x, \boldsymbol{\theta}) \in \partial\Omega \times \mathbf{S}^1 : \pm\nu(x)\cdot\boldsymbol{\theta} > 0\}$ the incoming (-), respectively outgoing (+), unit tangent sub-bundles of the boundary; where $\nu(x)$ is the outer unit normal at $x \in \partial\Omega$. Points (x_1, x_2) in the plane are identified by the complex numbers $z = x_1 + ix_2$, and directions $\boldsymbol{\theta} = (\cos\theta, \sin\theta)$ in the unit sphere $\mathbf{S}^1$ by $e^{i\theta}$.

Proposition 3.1. *Let* $\mathbf{F} \in H_0^s(\Omega;\mathbb{R}^2)$, $s \geqslant 1$. *The system*

$$\boldsymbol{\theta}\cdot\nabla u^0(z,\boldsymbol{\theta}) = \boldsymbol{\theta}\cdot\mathbf{F}(z), \quad \textit{for } (z,\boldsymbol{\theta}) \in \Omega\times\mathbf{S}^1, \tag{27a}$$

$$\boldsymbol{\theta}\cdot\nabla u^1(z,\boldsymbol{\theta}) = u^0(z,\boldsymbol{\theta}), \tag{27b}$$

subject to the boundary conditions

$$u^k|_{\Gamma_-} = 0, \quad k = 0,1, \tag{27c}$$

has a unique solution $u^k \in H^s(\Omega\times\mathbf{S}^1)$, $s \geqslant 1$. *In particular* $u^k|_{\Gamma\times\mathbf{S}^1} \in H^s(\mathbf{S}^1; H^{s-\frac{1}{2}}(\Gamma))$.

Moreover, $\langle u^0|_{\Gamma_+}, u^1|_{\Gamma_+}\rangle$ *are in a one-to-one correspondence with the Doppler transforms* $\langle D^0\mathbf{F}, D^1\mathbf{F}\rangle$ *in* (1) *and* (2) *via the relations*

$$\begin{aligned} u^0|_{\Gamma_+}(x,\boldsymbol{\theta}) &= D^0\mathbf{F}(x,\boldsymbol{\theta}),\\ u^1|_{\Gamma_+}(x,\boldsymbol{\theta}) &= (x\cdot\boldsymbol{\theta})u^0|_{\Gamma_+}(x,\boldsymbol{\theta}) - D^1\mathbf{F}(x,\boldsymbol{\theta}). \end{aligned} \tag{28}$$

Proof. From (27a) and (27b), we note that for $(x,\boldsymbol{\theta}) \in \Omega\times\mathbf{S}^1$,

$$\frac{d}{dt}\left[u^0(x+t\boldsymbol{\theta},\boldsymbol{\theta})\right] = \boldsymbol{\theta}\cdot\mathbf{F}(x+t\boldsymbol{\theta}), \quad \text{and} \quad \frac{d}{dt}\left[u^1(x+t\boldsymbol{\theta},\boldsymbol{\theta})\right] = u^0(x+t\boldsymbol{\theta},\boldsymbol{\theta}). \tag{29}$$

For $(x,\boldsymbol{\theta}) \in \Omega\times\mathbf{S}^1$ an integration along the line through x in the direction of $\boldsymbol{\theta}$ in (27a) together with the zero incoming condition (27c) yield

$$u^0(x,\boldsymbol{\theta}) = \int_{-\infty}^{x\cdot\boldsymbol{\theta}} \frac{d}{dt}u^0(\Pi_{\boldsymbol{\theta}}(x)+t\boldsymbol{\theta},\boldsymbol{\theta})dt = \int_{-\infty}^{x\cdot\boldsymbol{\theta}} \boldsymbol{\theta}\cdot\mathbf{F}(\Pi_{\boldsymbol{\theta}}(x)+t\boldsymbol{\theta})dt. \tag{30}$$

Similarly, a recursive integration by parts in (27b) together with (27c) yield

$$\begin{aligned} u^1(x,\boldsymbol{\theta}) &= \int_{-\infty}^{x\cdot\boldsymbol{\theta}} \frac{d}{dt}u^1(\Pi_{\boldsymbol{\theta}}(x)+t\boldsymbol{\theta},\boldsymbol{\theta})dt = \int_{-\infty}^{x\cdot\boldsymbol{\theta}} u^0(\Pi_{\boldsymbol{\theta}}(x)+t\boldsymbol{\theta},\boldsymbol{\theta})dt\\ &= (x\cdot\boldsymbol{\theta})u^0(x,\boldsymbol{\theta}) - D^1\mathbf{F}(x,\boldsymbol{\theta}), \end{aligned} \tag{31}$$

where the last equality uses the fact that $\mathbf{F}(x+(t-x\cdot\boldsymbol{\theta})\boldsymbol{\theta}) = 0$ for every $(x,\boldsymbol{\theta}) \in \Gamma_+$ and $t > x\cdot\boldsymbol{\theta}$. The relations (28) now follow from (30) and (31).

Since $\mathbf{F} \in H_0^s(\Omega;\mathbb{R}^2)$, $s \geqslant 1$, the solution u^0 given by (30) preserves the regularity and $u^0 \in H^s(\Omega\times\mathbf{S}^1)$, $s \geqslant 1$. Moreover, by (27b) and (31), $u^1 \in H^s(\Omega\times\mathbf{S}^1)$, $s \geqslant 1$. □

In our inverse problem, the solution (u^0,u^1) of the boundary value problem (27) is unknown in Ω, since $\mathbf{F}$ is unknown. However, their traces

$$g^k = \begin{cases} u^k|_{\Gamma_+} & \text{on } \Gamma_+,\\ 0 & \text{on } \Gamma_-, \end{cases} \quad k = 0,1, \tag{32}$$

are known on $\Gamma\times\mathbf{S}^1$ from the Doppler data via (28).

While unknown, the smoothness assumption on $\mathbf{F}$ yield $u^k \in H^2(\Omega\times\mathbf{S}^1)$ and $g^k \in H^2(\mathbf{S}^1; H^{3/2}(\Gamma))$ for $k = 0,1$. Consequently, $D^0\mathbf{F}, D^1\mathbf{F} \in H^2(\mathbf{S}^1; H^{3/2}(\Gamma))$.

We use the Fourier approach to the transport problem and work with the sequence of the (non-positive) Fourier coefficients of $u^k(z,\cdot)$,

$$u_n^k(z) = \frac{1}{2\pi}\int_{-\pi}^{\pi} u^k(z,\boldsymbol{\theta})e^{-\mathrm{i}n\theta}d\theta, \ n \leqslant 0, \ k = 0,1.$$

For $\theta = \arg \boldsymbol{\theta} \in (-\pi, \pi]$, the advection operator $\boldsymbol{\theta} \cdot \nabla = e^{-i\theta}\overline{\partial} + e^{i\theta}\partial$, where $\overline{\partial}$ and ∂ are Cauchy-Riemann operators in (10). By identifying the Fourier coefficients in the system (27a) and (27b), the solution u^k_{-n}'s solve

$$\overline{\partial} u^0_0(z) + \partial u^0_{-2}(z) = f_1(z), \tag{33}$$

$$\overline{\partial} u^0_{-n}(z) + \partial u^0_{-n-2}(z) = 0, \qquad n \geqslant 1, \tag{34}$$

$$\overline{\partial} u^1_{-n}(z) + \partial u^1_{-n-2}(z) = u^0_{-n-1}(z), \quad n \in \mathbb{Z}, \tag{35}$$

and

$$u^k_{-n}|_{\Gamma} = g^k_{-n}, \tag{36}$$

where

$$f_1 := \frac{1}{2}(F_1 + \mathrm{i}F_2). \tag{37}$$

The existence of the solution to the boundary value problem (33) - (36) is postulated by the forward problem.

For $k = 0, 1$, let $\mathbf{u}^k$ be the sequence valued map of the Fourier coefficients of the solution u^k and $\mathbf{g}^k$ be its corresponding trace on the boundary:

$$\mathbf{u}^k(z) = \langle u^k_0(z), u^k_{-1}(z), u^k_{-2}(z), u^k_{-3}(z), \cdots \rangle, \quad z \in \Omega, \tag{38}$$

$$\mathbf{g}^k = \langle g^k_0, g^k_{-1}, g^k_{-2}, g^k_{-3}, \cdots \rangle := \mathbf{u}^k|_{\Gamma}. \tag{39}$$

Since $u^k \in H^2(\mathbf{S}^1; H^2(\Omega))$, $\mathbf{u}^k \in l^{2,2}(\mathbb{N}; H^2(\Omega))$ and $\mathbf{g}^k \in l^{2,2}(\mathbb{N}; H^{\frac{3}{2}}(\Gamma))$.

In the sequence valued map notation the boundary value problem (33) - (36) becomes

$$\overline{\partial} L\mathbf{u}^0 + L^2 \partial L\mathbf{u}^0 = \mathbf{0}, \tag{40a}$$

$$\overline{\partial} \mathbf{u}^1 + L^2 \partial \mathbf{u}^1 = L\mathbf{u}^0, \tag{40b}$$

subject to

$$\mathbf{g}^k = \mathbf{u}^k|_{\Gamma}, \quad \text{for } k = 0, 1, \tag{40c}$$

where $L\mathbf{u}^0 = \langle u^0_{-1}, u^0_{-2}, u^0_{-3}, \cdots \rangle$ is the shifted sequence valued map.

Since $L\mathbf{u}^0$ is L^2-analytic, the Bukhgeim-Cauchy Integral formula (68) determines the sequence $L\mathbf{u}^0$ inside Ω from its boundary values:

$$L\mathbf{u}^0 = \mathcal{B}(L\mathbf{g}^0). \tag{41}$$

Componentwise, for $n \geqslant 1$,

$$u^0_{-n}(z) = \frac{1}{2\pi i}\int_{\Gamma} \frac{g^0_{-n}(\zeta)}{\zeta - z} d\zeta + \frac{1}{2\pi i}\int_{\Gamma} \left\{ \frac{d\zeta}{\zeta - z} - \frac{d\overline{\zeta}}{\overline{\zeta} - \overline{z}} \right\} \sum_{j=1}^{\infty} g^0_{-n-2j}(\zeta) \left(\frac{\overline{\zeta} - \overline{z}}{\zeta - z} \right)^j, \ z \in \Omega. \tag{42}$$

Applying Theorem 2.1 (for $\mathbf{v} = \mathbf{u}^0$ and $\mathbf{w} = \mathbf{0}$ therein) to the boundary value problem (40a) and (40c), and using estimate (11) yields

$$\left\| L\mathbf{u}^0 \right\|^2_{p,1} \lesssim \left\| L\mathbf{g}^0 \right\|^2_{p+\frac{1}{2},\frac{1}{2}}, \quad \text{for } 0 \leqslant p \leqslant 1. \tag{43}$$

Next, we show that the additional momentum data g^1 recovers the real valued mode u^0_0.

Since the modes $\langle u^0_{-1}, u^0_{-2}, u^0_{-3}, \cdots \rangle$ are now recovered in Ω by (42), the right hand side of the non-homogenous Bukhgeim Beltrami system (35) is known. The solution of (35) is given by the explicit

Pompeiu-like formula (75) for the $(\overline{\partial} - L^2\partial)$ operator; see the Appendix B for a derivation. In the reconstruction, we recover the mode u^1_{-1} from the first component of (75), namely

$$
\begin{aligned}
u^1_{-1}(z) := \frac{1}{2\pi \mathrm{i}} \int_\Gamma \frac{g^1_{-1}(\zeta)}{\zeta - z} d\zeta + \frac{1}{2\pi \mathrm{i}} \int_\Gamma \left\{ \frac{d\zeta}{\zeta - z} - \frac{d\overline{\zeta}}{\overline{\zeta} - \overline{z}} \right\} \sum_{j=1}^{\infty} g^1_{-1-2j}(\zeta) \left(\frac{\overline{\zeta} - \overline{z}}{\zeta - z} \right)^j \\
- \frac{1}{\pi} \sum_{j=0}^{\infty} \int_\Omega \frac{u^0_{-2-2j}(\zeta)}{\zeta - z} \left(\frac{\overline{\zeta} - \overline{z}}{\zeta - z} \right)^j d\xi d\eta, \qquad \zeta = \xi + i\eta, \quad z \in \Omega.
\end{aligned} \tag{44}
$$

The Fourier mode u^0_0 is determined by

$$
u^0_0(z) := 2\,\mathbb{R}\mathrm{e}\,\partial u^1_{-1}(z), \quad z \in \Omega, \tag{45}
$$

with the estimate

$$
\left\| u^0_0 \right\|^2_{H^1(\Omega)} \lesssim \left\| u^1_{-1} \right\|^2_{H^2(\Omega)} \lesssim \left\| \mathbf{u}^1 \right\|^2_{0,2}. \tag{46}
$$

Applying Theorem 2.2 part (b) to the boundary value problem (40b)-(40c), and using (19) yields

$$
\left\| \mathbf{u}^1 \right\|^2_{0,2} \lesssim \left\| L\mathbf{u}^0 \right\|^2_{1,1} + \left\| L\mathbf{g}^0 \right\|^2_{\frac{3}{2},\frac{1}{2}} + \left\| \mathbf{g}^1 \right\|^2_{\frac{3}{2},\frac{3}{2}}. \tag{47}
$$

From mode u^0_{-2} in (42) and mode u^0_0 in (45), we use (33) to recover

$$
f_1(z) := \partial u^0_{-2}(z) + \overline{\partial} u^0_0(z), \quad z \in \Omega, \tag{48}
$$

and define the vector field

$$
\mathbf{F}(z) := \langle 2\,\mathbb{R}\mathrm{e}\, f_1(z), 2\,\mathbb{I}\mathrm{m}\, f_1(z) \rangle. \tag{49}
$$

Furthermore, the following estimate holds:

$$
\begin{aligned}
\|\mathbf{F}\|^2_{L^2(\Omega)} &\lesssim \left\| u^0_{-2} \right\|^2_{H^1(\Omega)} + \left\| u^0_0 \right\|^2_{H^1(\Omega)} \\
&\lesssim \left\| L\mathbf{u}^0 \right\|^2_{0,1} + \left\| u^0_0 \right\|^2_{H^1(\Omega)} \\
&\lesssim \left\| L\mathbf{u}^0 \right\|^2_{0,1} + \left\| \mathbf{u}^1 \right\|^2_{0,2} \\
&\lesssim \left\| L\mathbf{u}^0 \right\|^2_{0,1} + \left\| L\mathbf{u}^0 \right\|^2_{1,1} + \left\| L\mathbf{g}^0 \right\|^2_{\frac{3}{2},\frac{1}{2}} + \left\| \mathbf{g}^1 \right\|^2_{\frac{3}{2},\frac{3}{2}} \\
&\lesssim \left\| L\mathbf{g}^0 \right\|^2_{\frac{1}{2},\frac{1}{2}} + \left\| L\mathbf{g}^0 \right\|^2_{\frac{3}{2},\frac{1}{2}} + \left\| \mathbf{g}^1 \right\|^2_{\frac{3}{2},\frac{3}{2}} \\
&\lesssim \left\| L\mathbf{g}^0 \right\|^2_{\frac{3}{2},\frac{1}{2}} + \left\| \mathbf{g}^1 \right\|^2_{\frac{3}{2},\frac{3}{2}} \lesssim \left\| D^0\mathbf{F} \right\|^2_{\frac{3}{2},\frac{1}{2}} + \left\| D^1\mathbf{F} \right\|^2_{\frac{3}{2},\frac{3}{2}}
\end{aligned} \tag{50}
$$

where the third inequality uses (46), the fourth inequality uses (47), and the fifth inequality uses (43). □

4. Numerical Implementation

In this section we present the reconstruction results obtained by the numerical implementation of the proof of Theorem 1.1. The Doppler data is simulated for two specific vector fields sharing the same solenoidal part, while the reconstruction from both noiseless and noisy data is performed for each vector field. The domain Ω is the unit disk centered at the origin and its boundary Γ is the unit circle.

Starting from a vector field $\mathbf{F}$, the data is computed by numerical integration in (1) and (2) via the composite mid-point rule along lines. The data is calculated at $1{,}440$ boundary points $x \in \Gamma$ of equal angular spacing, and at about 720 equiangular outgoing directions $\boldsymbol{\theta} \in \mathbf{S}^1$ (satisfying $x \cdot \boldsymbol{\theta} > 0$).

To avoid an inverse crime, the reconstruction algorithm uses a different numerical path: each component of the vector field is recovered as a piecewise constant approximation on a ($1{,}750$ elements) triangular partition of Ω. We use (42) to compute the values of u^0_{-n} at the vertices of the partition, yielding a piecewise linear approximation to u^0_{-n}. More precisely, if $u^0_{-n} \approx ax_1 + bx_2 + c$ on a triangle τ, then $\partial u^0_{-n}|_\tau \approx \dfrac{1}{2}(a - b\mathrm{i})$ as a piecewise constant approximation required in (48). In contrast, the mode u^1_{-1} is computed at each centroid by (44). More precisely, at the centroid c of each triangle τ,

$$\begin{aligned} u^1_{-1}(c+\lambda) \approx & u^1_{-1}(c) + \partial_{x_1} u^1_{-1}(c)\lambda_1 + \partial_{x_2} u^1_{-1}(c)\lambda_2 \\ & + \frac{1}{2}\partial^2_{x_1x_1} u^1_{-1}(c)\lambda_1^2 + \partial^2_{x_1x_2} u^1_{-1}(c)\lambda_1\lambda_2 + \frac{1}{2}\partial^2_{x_2x_2} u^1_{-1}(c)\lambda_2^2 \end{aligned}$$

for small $\lambda = (\lambda_1, \lambda_2)$. We write τ_1, τ_2, $\ldots$, τ_K the triangles sharing vertices or edges with τ. Then substituting $\lambda = c - c_k$, $k = 1, 2, \ldots, K$ to the expansion, we obtain K linear constraints with five unknowns $\partial_{x_1} u^1_{-1}(c)$, $\partial_{x_2} u^1_{-1}(c)$, $\partial^2_{x_1x_1} u^1_{-1}(c)$, $\partial^2_{x_1x_2} u^1_{-1}(c)$, and $\partial^2_{x_2x_2} u^1_{-1}(c)$ required in (48) with (45) to find $\overline{\partial} u^0_0$. The least square method leads a unique solution to them on each τ. Note that the singularity of the integrand of the final term in (44) is removable and a conoventional numerical integral rule can be applied.

Throughout this section, the series in (42) and (44) are truncated up to 256 Fourier modes. The truncation index not only controls the accuracy, but also plays a regularizing role in stability.

In the examples below, the relative errors between the reconstructed vector field $\mathbf{F}_{\text{recon}}$ and the exact $\mathbf{F}$ are in the L^2 sense :

$$\|\mathbf{F}_{\text{recon}} - \mathbf{F}\|_{\text{rel}} = \frac{\|\mathbf{F}_{\text{recon}} - \mathbf{F}\|_2}{\|\mathbf{F}\|_2}. \tag{51}$$

Similarly, the relative error in the data is in the L^2 sense.

All numerically reconstructed results are calculated in the double precision arithmetic on AMD EPYC 7643 with 96 threads OpenMP parallel computations.

Example 1. We consider first the vector field

$$\mathbf{F}(x) = \nabla\left(\sin\pi|x|^2\right) + \mathbf{F}^s(x), \tag{52}$$

where the solenoidal part

$$\mathbf{F}^s(x) = \begin{pmatrix} 2x_1x_2\cos|x|^2 + \cos(6x_1x_2) - 6x_1x_2\sin(6x_1x_2) \\ -\sin|x|^2 - 2x_1^2\cos|x|^2 + 6x_1x_2\sin(6x_1x_2) \end{pmatrix}; \tag{53}$$

see Figure 2.

Example 1(a) - Noiseless data: For the vector field $\mathbf{F}$ in (52), the simulated data $(D^0\mathbf{F}, D^1\mathbf{F})$ is illustrated in Figure 1, where crosses ($\times$) depict a few boundary nodes $x \in \Gamma$, while the red and blue curves are $\{x + |D^j\mathbf{F}(x,\boldsymbol{\theta})|\boldsymbol{\theta}\,;\, \boldsymbol{\theta} \in \mathbf{S}^1, x\cdot\boldsymbol{\theta} > 0\}$, $j = 0, 1$. Also, for illustration purposes, the radial direction is shrunk by $1/5$-th.

Note that $D^0\mathbf{F}$ and $D^1\mathbf{F}$ are not always positive. To differentiate the sign, the positive and negative parts are drawn in red, respectively in blue. Since only outgoing signals are measured (while the incoming flow is zero at the boundary) signals are depicted outside Ω only.

The numerically reconstructed result shown in Figure 3 has an relative error of 18.1%. The total elapsed time in the reconstruction is approximately 10 seconds.

Example 1(b) - Perturbed data within the range: To illustrate the stability estimate in Theorem 1.1, we first consider the case of data perturbed within the range. To generate such a data we solve the forward problem by (1) and (2) for a perturbed vector field $\mathbf{F}_\epsilon = \mathbf{F} + \epsilon$, for some smooth vector field

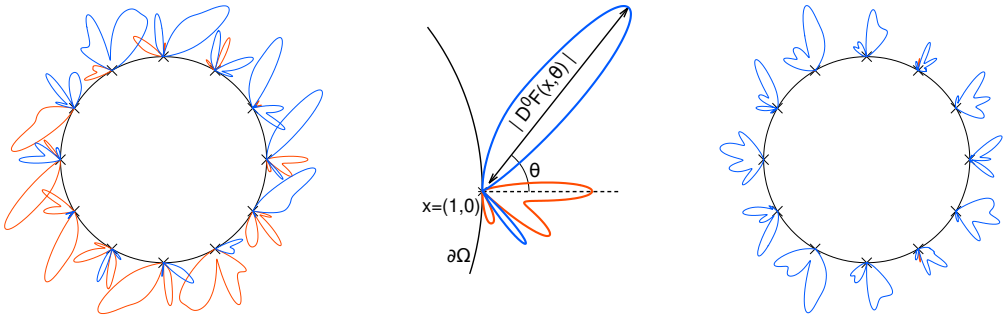

FIGURE 1. Simulated data for $\mathbf{F}$ in (52): $D^0\mathbf{F}$ (left) with its magnification at $x = (1,0)$ (middle), and $D^1\mathbf{F}$ (right). The crosses ($\times$) are some data collection points at the boundary, while the red and blue curves represent $D^j\mathbf{F}(x,\boldsymbol{\theta})$, $j = 0,1$ in polar coordinates $\big(|D^j\mathbf{F}(x,\boldsymbol{\theta})|,\boldsymbol{\theta}\big)$ centered at the respective boundary point $x \in \Gamma$. The radial direction is shrunk by $1/5$-th for illustration purposes.

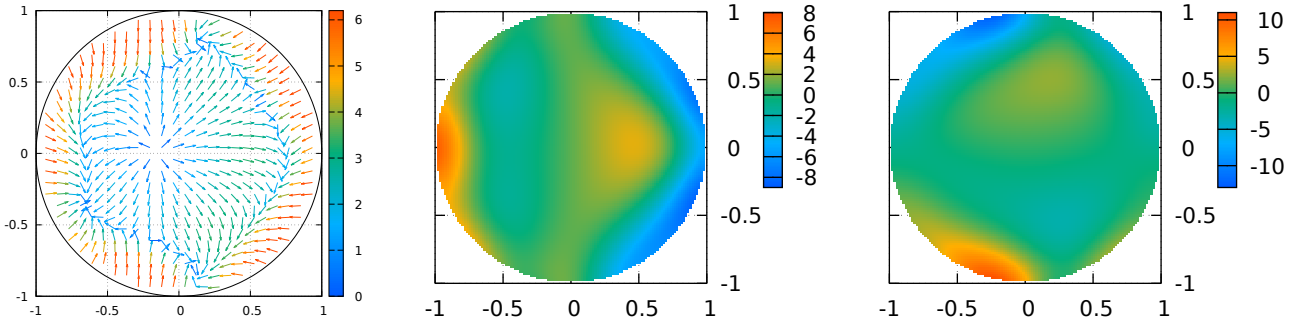

FIGURE 2. Exact vector field $\mathbf{F} = \langle F_1, F_2\rangle$ in (52) (left), its first component F_1 (middle) and its second component F_2 (right).

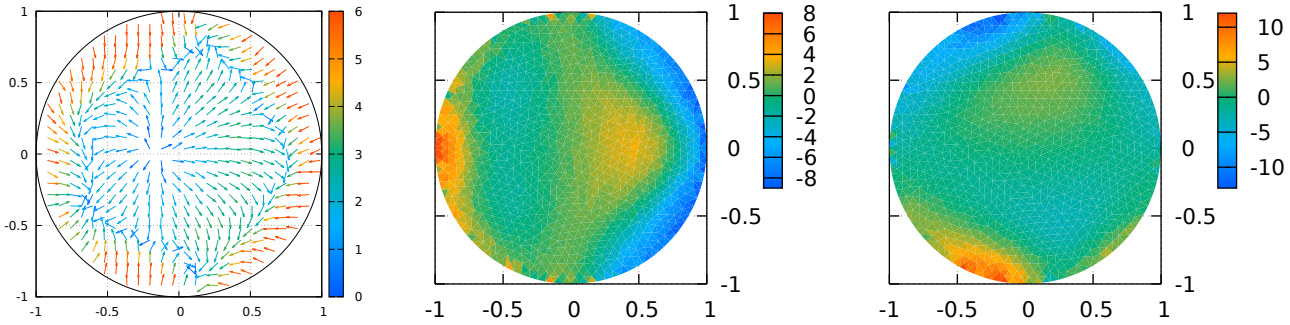

FIGURE 3. Numerical reconstruction from noiseless data: The vector field $\mathbf{F}_{0,\text{recon}}$ (left), its first component F_1 (middle) and its second component F_2 (right).

ϵ in Ω. Figure 4 below shows the reconstruction $\mathbf{F}_{\epsilon,\text{recon}}$ from this data. In this example, the relative error in the data for $D^0\mathbf{F}$ is 5.52% and for $D^1\mathbf{F}$ is 4.48%, while the relative error in the reconstruction is 30.0% error.

Example 1(c) - Noisy data : To assess the robustness of the method, we consider the same vector field as in (52), where the data is corrupted with an additive random error. Specifically, $D^0\mathbf{F}$ now

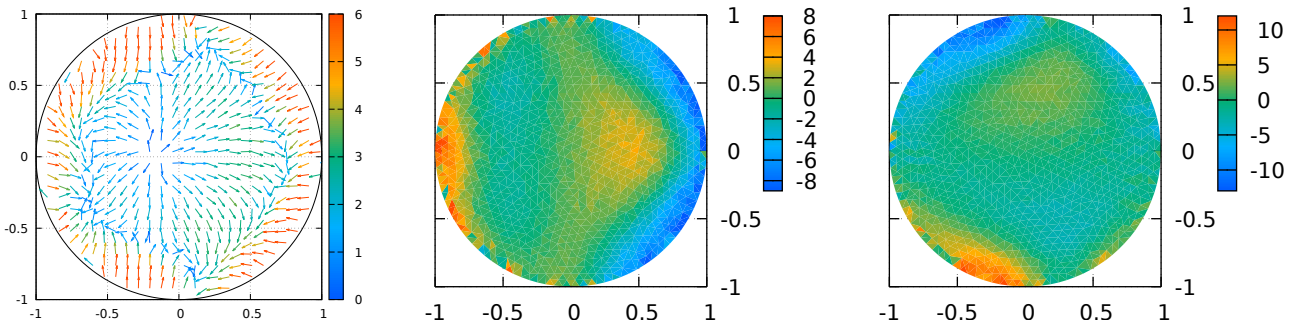

FIGURE 4. Numerical reconstruction from perturbed data within the range (5.52% relative error in $D^0\mathbf{F}$ and 4.48% in $D^1\mathbf{F}$). The reconstructed field $\mathbf{F}_{\epsilon,\text{recon}} = \langle F_1, F_2\rangle$ (left) and its components F_1 (middle) and F_2 (right) has 30.0% relative error.

contains about 5.88% relative error, while $D^1\mathbf{F}$ contains 4.34% relative error, which are at the same level as in the previous example; see Figure 5 for an illustration.

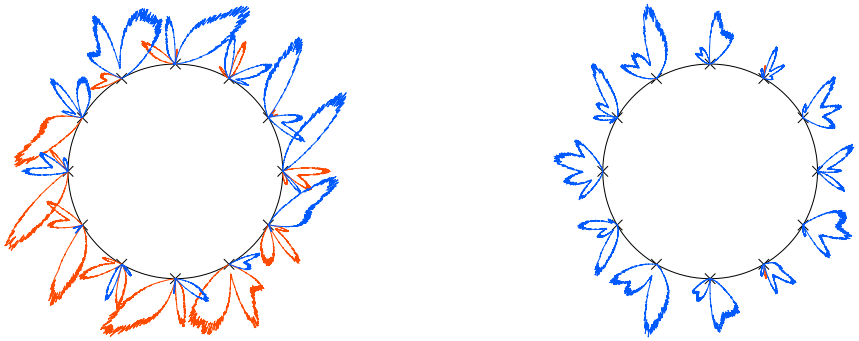

FIGURE 5. Noisy data $D^0\mathbf{F}$ (left) with 5.88% error and $D^1\mathbf{F}$ (right) with 4.34% error.

The reconstructed vector field $\mathbf{F}_{\text{recon}}$ shown in Figure 6, contains approximately 54.6% relative error.

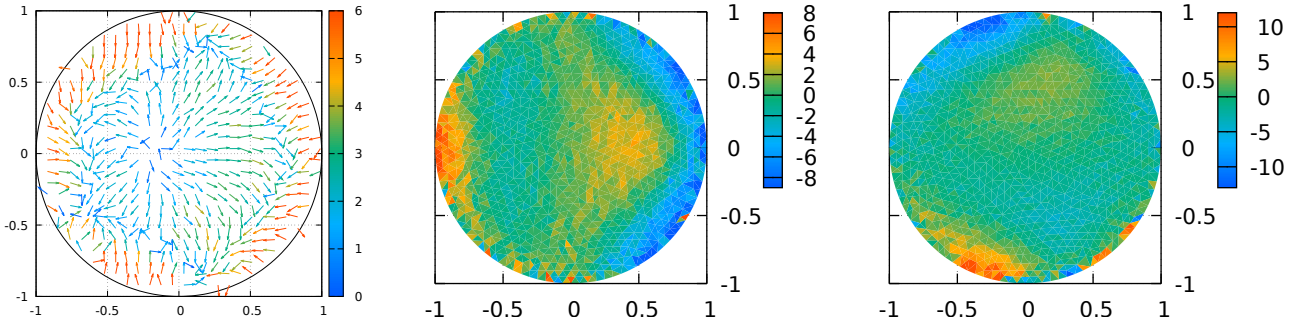

FIGURE 6. Numerical reconstruction from noisy data (5.88% relative error in $D^0\mathbf{F}$ and 4.34% in $D^1\mathbf{F}$). The reconstructed field $\mathbf{F}_{\text{recon}} = \langle F_1, F_2\rangle$ (left) and its components F_1 (middle) and F_2 (right) has 54.6% relative error.

Example 2. We consider next the vector field

$$\mathbf{F}(x) = \nabla\left(\arctan\frac{x_2}{2+x_1}\right) + \mathbf{F}^s(x) \tag{54}$$

with the same solenoidal part $\mathbf{F}^s$ as in (53).

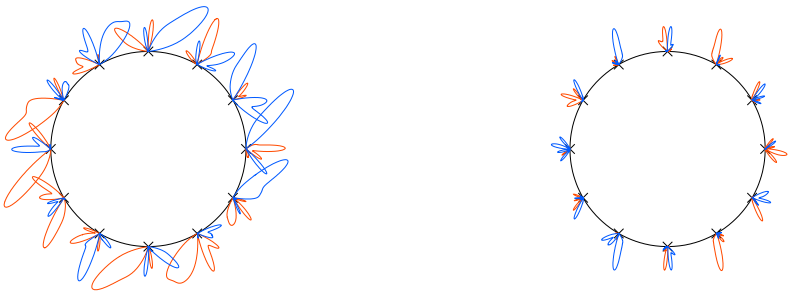

FIGURE 7. Simulated noiseless data $D^0\mathbf{F}$ (left) and $D^1\mathbf{F}$ (right) for $\mathbf{F}$ in (54). The crosses ($\times$) are some data collection points at the boundary, while the red and blue curves represent $D^j\mathbf{F}(x,\boldsymbol{\theta})$, $j=0,1$ in polar coordinates $\left(|D^j\mathbf{F}(x,\boldsymbol{\theta})|,\boldsymbol{\theta}\right)$ centered at the respective boundary point $x\in\Gamma$.

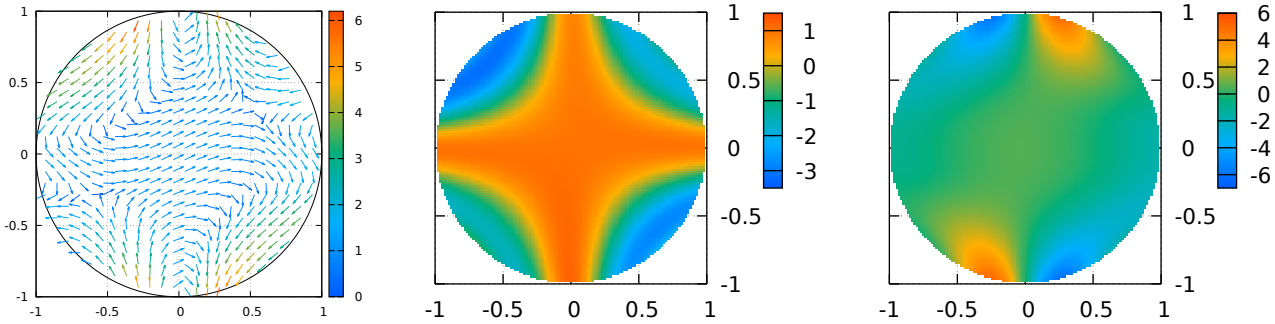

FIGURE 8. Exact vector field $\mathbf{F}=\langle F_1,F_2\rangle$ in (54) (left), its first component F_1 (middle) and its second component F_2 (right).

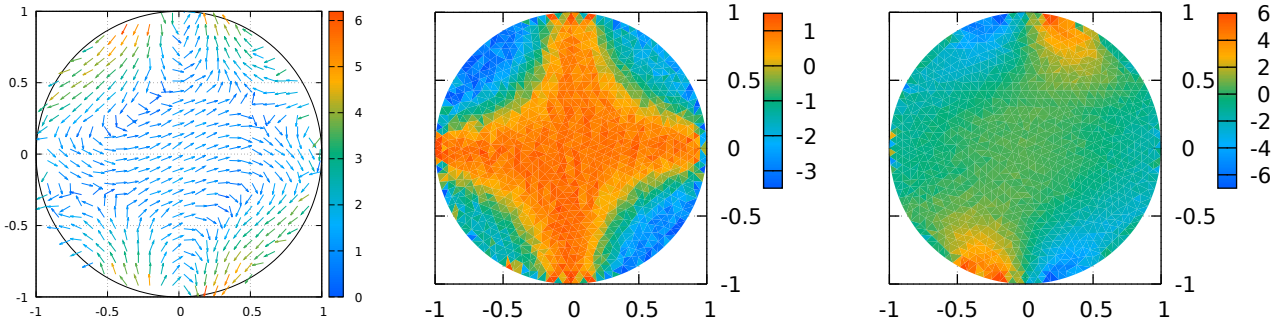

FIGURE 9. Numerically reconstructed vector field from noiseless Doppler data: vector field $\mathbf{F}_{0,\text{recon}}=\langle F_1,F_2\rangle$ (left) and its components F_1 (middle) and F_2 (right).

Example 2(a) - Noiseless data: The vector field in (54) is depicted in Figure 8, while its corresponding simulated Doppler data is shown in Figure 7. The numerically reconstructed vector field and its components are exhibited in Figure 9 having 31.1% relative error.

Example 2(b) - Perturbed data within the range: In this case, the generated perturbed data $\mathbf{F}_\epsilon$ depicted in Figure 10 has 5.02% relative error in $D^0\mathbf{F}$ and 6.04% relative error in $D^1\mathbf{F}$. The numerical reconstruction of $\mathbf{F}_{\epsilon,\text{recon}}$ in Figure 11 has 45.9% relative error.

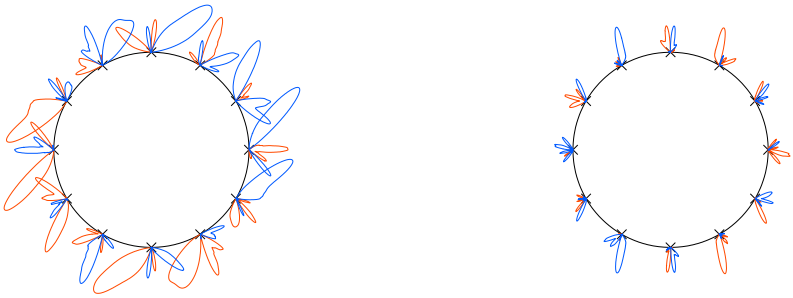

FIGURE 10. Data $D^0\mathbf{F}_\epsilon$ (left) with 5.02% error and $D^1\mathbf{F}_\epsilon$ (right) with 6.04% error, which is considered as measurement data with noise in range

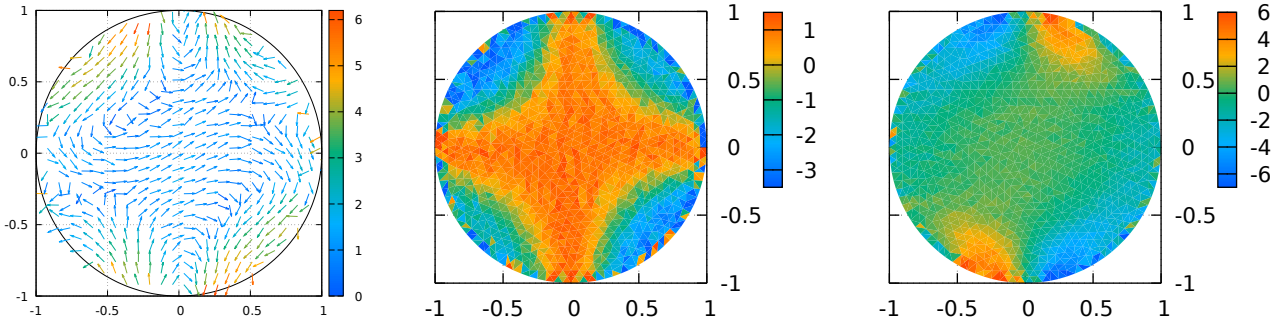

FIGURE 11. Numerical reconstruction from perturbed data within the range (5.02% relative error in $D^0\mathbf{F}$ and 6.04% in $D^1\mathbf{F}$). The reconstructed field $\mathbf{F}_{\epsilon,\text{recon}} = \langle F_1, F_2 \rangle$ (left) and its components F_1 (middle) and F_2 (right) has 45.9% relative error.

Example 2(c) - Noisy data: We consider the same vector field as in (54), however the data is corrupted with additive random errors: 6.03% relative error in $D^0\mathbf{F}$, and 5.04% in $D^1\mathbf{F}$.

The numerical reconstruction results are shown in Figure 12. The reconstructed vector field $\mathbf{F}_{\text{recon}}$ has 71.3% relative error.

In Table 1 below, we summarize the level of error obtain in the examples. The reconstruction error in Example 1(b) (30.0%), respectively, Example 2(b) (45.9%) obtained from the perturbed data within the range reflects the instability of our method due to twice differentiation. The reconstruction error in Example 1(c) (54.6%), respectively, Example 2(c) (71.3%) obtained from (an additive random error) noisy data is also due to the ill-posedness (non-existence) specific to inverting data outside the range.

ACKNOWLEDGMENT

The work of H. Fujiwara was supported by JSPS KAKENHI Grant Numbers JP20H01821, JP21H00999 and JP22K18674. The work of D. Omogbhe was supported by the Austrian Science Fund (FWF), Project P31053-N32, and by the FWF Project F6801–N36 within the Special Research Program SFB F68 "Tomography Across the Scales". The work of K. Sadiq was supported by the Austrian Science Fund (FWF), Project P31053-N32. The work of A. Tamasan was supported in part by the National Science Foundation DMS-1907097.

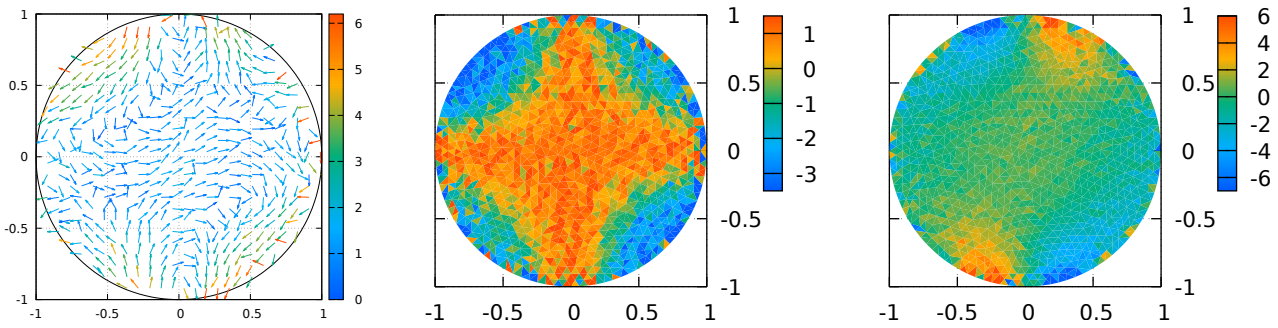

FIGURE 12. Numerical reconstruction from noisy data (6.03% relative error in $D^0\mathbf{F}$ and 5.04% in $D^1\mathbf{F}$). The reconstructed field $\mathbf{F}_{\text{recon}} = \langle F_1, F_2 \rangle$ (left) and its components F_1 (middle) and F_2 (right) has 71.3% relative error.

TABLE 1. Differences between perturbed data in the range and additive random noise.

Relative error in	Example 1 (b) Perturbed data in the range	Example 1 (c) Random noise	Example 2 (b) Perturbed data in the range	Example 2 (c) Random noise
$D^0\mathbf{F}$	5.52%	5.88%	5.02%	6.03%
$D^1\mathbf{F}$	4.48%	4.34%	6.04%	5.04%
Reconstruction	30.0%	54.6%	45.9%	71.3%

APPENDIX A. A HIERACHY OF NORMS INDUCED BY THE LEFT TRANSLATION

For sequence valued maps with elements in a Banach space $(B, \|\cdot\|)$, we introduce here a hierarchy of norms compatible with the left translation operator.

Recall the notation $\|\mathbf{v}\| \lesssim \|\mathbf{w}\|$, whenever $\|\mathbf{v}\| \leqslant C \|\mathbf{w}\|$ for some constant $C > 0$ independent of $\mathbf{v}$ and $\mathbf{w}$. We also denote $\|\mathbf{v}\| \approx \|\mathbf{w}\|$ if $\|\mathbf{v}\| \lesssim \|\mathbf{w}\| \lesssim \|\mathbf{v}\|$.

We define inductively the spaces $l^{2,\frac{p}{2}}(\mathbb{N}; B)$, for $p \geqslant 0$ integer as follows:
$l^{2,0}(\mathbb{N}; B)$ is the space of sequences $\mathbf{u}$ with

$$\|\mathbf{u}\|_0 := \left(\sum_{j=0}^{\infty} \|u_j\|^2 \right)^{\frac{1}{2}} < \infty, \tag{55}$$

while for $p \geqslant 1$, we define

$$l^{2,\frac{p}{2}}(\mathbb{N}; B) := \left\{ \mathbf{u} = \langle u_0, u_{-1}, u_{-2}, \cdots \rangle : \|\mathbf{u}\|_{\frac{p}{2}} < \infty \right\}, \tag{56}$$

where

$$\|\mathbf{u}\|_{\frac{p}{2}} := \left(\sum_{n=0}^{\infty} \|L^n \mathbf{u}\|^2_{\frac{p-1}{2}} \right)^{\frac{1}{2}}. \tag{57}$$

The following result shows the equivalence of the norm in (57) with the weighted l^2-norms.

Lemma A.1. *Let $(B, \|\cdot\|)$ be a Banach space, and $\mathbf{u} \in l^{2,\frac{p}{2}}(\mathbb{N}; B)$, for some $p \geqslant 0$ integer. Then*

$$\|\mathbf{u}\|^2_{\frac{p}{2}} = \sum_{j=0}^{\infty} \binom{j+p}{p} \|u_j\|^2 \approx \sum_{j=0}^{\infty} (1+j)^p \|u_j\|^2, \tag{58}$$

where $\binom{j+p}{p} = \dfrac{(j+p)!}{j!p!}$.

Proof. We first show the equality in (58) by induction in p.

The case $p = 0$ holds by definition (55).

Assume next that the equality in (58) holds for some fixed p:

$$\|\mathbf{u}\|^2_{\frac{p}{2}} = \sum_{j=0}^{\infty} \binom{j+p}{p} \|u_j\|^2. \tag{59}$$

By definition (57),

$$\|\mathbf{u}\|^2_{\frac{p+1}{2}} = \sum_{n=0}^{\infty} \|L^n \mathbf{u}\|^2_{\frac{p}{2}} = \sum_{m=0}^{\infty} \sum_{n=0}^{\infty} \binom{m+p}{p} \|u_{m+n}\|^2. \tag{60}$$

By changing the index $j = m + n$, for $m \geqslant 0$, ($j - n \geqslant 0$, and $n \leqslant j$) we get

$$\sum_{m=0}^{\infty} \sum_{n=0}^{\infty} \binom{m+p}{p} \|u_{m+n}\|^2 = \sum_{j=0}^{\infty} \sum_{n=0}^{j} \binom{j-n+p}{p} \|u_j\|^2 = \sum_{j=0}^{\infty} \|u_j\|^2 \sum_{n=0}^{j} \binom{j-n+p}{p}. \tag{61}$$

Note that for fixed j, by changing the index $k = j - n + p$, and using Pascal's recurrence,

$$\begin{aligned} \sum_{n=0}^{j} \binom{j-n+p}{p} &= \sum_{k=p}^{j+p} \binom{k}{p} = \sum_{k=p}^{j+p} \binom{k+1}{p+1} - \sum_{k=p}^{j+p} \binom{k}{p+1} \\ &= \sum_{k=p+1}^{j+p+1} \binom{k}{p+1} - \sum_{k=p}^{j+p} \binom{k}{p+1} \\ &= \binom{j+p+1}{p+1}, \end{aligned} \tag{62}$$

where in the last equality we use a telescoping argument. Thus, using (62) and (61), the expression in (60) yields

$$\|\mathbf{u}\|^2_{\frac{p+1}{2}} = \sum_{j=0}^{\infty} \binom{j+p+1}{p+1} \|u_j\|^2.$$

The equivalence of the norm in (58) follows from the inequalities

$$\frac{1}{p!}(1+j)^p \leqslant \binom{j+p}{p} \leqslant (1+j)^p.$$

□

The following result recalls the extension of the resolvent of the left translation operator L from outside the unit disc to the unit circle.

Lemma A.2. *Let* $\mathbf{a} \in l^2$, $\mathbf{c} \in l^{2,1}$ *be sequences,* L *be the left translation operator, and* $\lambda \in \mathbb{C}$ *with* $|\lambda| \geqslant 1$. *If* $\mathbf{a}, \mathbf{c}$ *satisfy*

$$(\lambda - L)\mathbf{a} = \mathbf{c}, \tag{63}$$

then there exists an $M > 0$ *independent of* λ *such that*

$$\|\mathbf{a}\|_{l^2} \leqslant M \|\mathbf{c}\|_{l^{2,1}}. \tag{64}$$

For the proof of the estimate (64), we refer to [25, Lemma 3.1.1, Step 1].

Appendix B. An explicit Pompeiu formula for L^2-analytic maps

In here, we derive the Pompeiu type formula corresponding to A-analytic maps, which is used in the reconstruction method.

Bukhgeim's original theory in [3] considers the sequence valued maps

$$\Omega \ni z \mapsto \mathbf{u}(z) := \langle u_0(z), u_{-1}(z), u_{-2}(z), \cdots \rangle, \tag{65}$$

and solution of the Beltrami-like equation

$$\overline{\partial}\mathbf{u}(z) + L^2 \partial \mathbf{u}(z) = \mathbf{0}, \quad z \in \Omega, \tag{66}$$

where $L\mathbf{u}(z) = L(u_0(z), u_{-1}(z), u_{-2}(z), \cdots) := (u_{-1}(z), u_{-2}(z), \cdots)$ denotes the left translation. These solutions are called L^2-analytic.

Similar to classical analytic maps, the solution of (66) satisfy a Cauchy-like integral formula,

$$\mathbf{u}(z) = \mathcal{B}[\mathbf{u}|_\Gamma](z), \quad z \in \Omega, \tag{67}$$

where $\mathcal{B}$ is the Bukhgeim-Cauchy operator acting on $\mathbf{u}|_\Gamma$ defined component-wise [5] for $n \geqslant 0$ by

$$(\mathcal{B}\mathbf{u})_{-n}(z) := \frac{1}{2\pi i}\int_\Gamma \frac{u_{-n}(\zeta)}{\zeta - z} d\zeta + \frac{1}{2\pi i}\int_\Gamma \left\{ \frac{d\zeta}{\zeta - z} - \frac{d\overline{\zeta}}{\overline{\zeta} - \overline{z}} \right\} \sum_{j=1}^{\infty} u_{-n-2j}(\zeta) \left(\frac{\overline{\zeta} - \overline{z}}{\zeta - z} \right)^j, \; z \in \Omega. \tag{68}$$

We next give the solution of the Bukhgeim-Beltrami system, which leads to Bukhgeim-Pompeiu formula.

Solution of the Bukhgeim-Beltrami system :

$$\overline{\partial} u_{-n}(z) + \partial u_{-n-2}(z) = v_{-n-1}(z), \quad n \in \mathbb{Z}. \tag{69}$$

Assume that Ω is bounded convex set with C^1 boundary, and for $n \geqslant 0$, let

$$\sigma_{-n}(z, \varphi) = \sum_{j=0}^{\infty} u_{-n-2j}(z) e^{-i(n+2j)\varphi},$$

and $\sigma_{-n} \in C^1(\Omega) \cap C(\overline{\Omega})$. Let $z \in \Omega$ and $\zeta \in \overline{\Omega}$, we write the parametrization $\zeta(\varphi) = z + l(\varphi)e^{i\varphi}$. For $n \geqslant 0$, we have

$$\begin{aligned}
\sigma_{-n}(\zeta, \varphi) - \sigma_{-n}(z, \varphi) &= \int_0^l \frac{\partial \sigma_{-n}}{\partial t}(z + te^{i\varphi}, \varphi) dt = \int_0^l \Big(\frac{\partial \sigma_{-n}}{\partial \overline{z}} e^{-i\varphi} + \frac{\partial \sigma_{-n}}{\partial z} e^{i\varphi} \Big) dt \\
&= \int_0^l \left(\sum_{j=0}^{\infty} \frac{\partial u_{-n-2j}}{\partial \overline{z}} e^{-i(n+2j+1)\varphi} + \sum_{j=0}^{\infty} \frac{\partial u_{-n-2j}}{\partial z} e^{i(-n-2j+1)\varphi} \right) dt \\
&= \int_0^l \frac{\partial u_{-n}}{\partial z} e^{-i(n-1)\varphi} dt + \int_0^l \sum_{j=0}^{\infty} \Big(\overline{\partial} u_{-n-2j} + \partial u_{-n-2j-2} \Big) e^{-i(n+2j+1)\varphi} dt.
\end{aligned} \tag{70}$$

We obtain the Fourier coefficients u_{-n} in Ω for $n \geqslant 0$ as follows:

$$\begin{aligned} u_{-n}(z) &= \frac{1}{2\pi}\int_0^{2\pi} \sigma_{-n}(z,\varphi)e^{in\varphi}d\varphi \\ &= \frac{1}{2\pi}\int_0^{2\pi} \sigma_{-n}(\zeta,\varphi)e^{in\varphi}d\varphi - \frac{1}{2\pi}\int_0^{2\pi}\int_0^{l(\varphi)} \frac{\partial u_{-n}}{\partial z}\frac{1}{te^{-i\varphi}}tdtd\varphi \\ &\quad - \frac{1}{2\pi}\int_0^{2\pi}\int_0^{l(\varphi)} \sum_{j=0}^{\infty}\Big(\overline{\partial}u_{-n-2j} + \partial u_{-n-2j-2}\Big)e^{-2ij\varphi}\frac{1}{te^{i\varphi}}tdtd\varphi \\ &= \frac{1}{2\pi}\int_0^{2\pi}\sum_{j=0}^{\infty} u_{-n-2j}(\zeta)e^{-2ij\varphi}d\varphi - \frac{1}{2\pi}\int_\Omega \frac{\partial u_{-n}}{\partial z}\frac{1}{\overline{\zeta}-\overline{z}}dA \\ &\quad - \frac{1}{2\pi}\int_\Omega \sum_{j=0}^{\infty}\Big(\overline{\partial}u_{-n-2j} + \partial u_{-n-2j-2}\Big)e^{-2ij\varphi}\frac{1}{\zeta - z}dA \end{aligned} \tag{71}$$

where dA is the element of the area, and in the second equality we use (70).

From $\zeta = z + l(\varphi)e^{i\varphi}$ we get

$$e^{-2i\varphi} = \frac{\overline{\zeta}-\overline{z}}{\zeta - z}, \qquad d\varphi = \frac{1}{2i}\left(\frac{1}{\zeta - z}d\zeta - \frac{1}{\overline{\zeta}-\overline{z}}d\overline{\zeta}\right), \tag{72}$$

and by the conjugate form of the Cauchy- Pompeiu formula (e.g. see [28]), we have

$$\frac{1}{2\pi}\int_\Omega \frac{\partial u_{-n}}{\partial \overline{z}}\frac{1}{\overline{\zeta}-z}dA = \frac{1}{2}u_{-n}(z) + \frac{1}{4\pi i}\int_{\partial\Omega} u_{-n}(\zeta)\frac{1}{\overline{\zeta}-\overline{z}}. \tag{73}$$

Substituting (72), (73) and (69) into (71) yields an explicit form of the Bukhgeim-Pompeiu formula [3], defined component-wise for $n \geqslant 0$ by

$$\begin{aligned} u_{-n}(z) &= \frac{1}{2\pi i}\int_\Gamma \frac{u_{-n}(\zeta)}{\zeta - z}d\zeta + \frac{1}{2\pi i}\int_\Gamma \left\{\frac{d\zeta}{\zeta - z} - \frac{d\overline{\zeta}}{\overline{\zeta}-\overline{z}}\right\}\sum_{j=1}^{\infty} u_{-n-2j}(\zeta)\left(\frac{\overline{\zeta}-\overline{z}}{\zeta - z}\right)^j \\ &\quad - \frac{1}{\pi}\sum_{j=0}^{\infty}\int_\Omega v_{-n-2j-1}(\zeta)\frac{1}{\zeta - z}\left(\frac{\overline{\zeta}-\overline{z}}{\zeta - z}\right)^j d\xi d\eta, \quad \zeta = \xi + i\eta. \end{aligned} \tag{74}$$

The following (75) is the Bukhgeim-Pompeiu formula, given in [3], and in an explicit form, defined component-wise for $n \geqslant 0$ by

$$\mathbf{u}_{-n}(z) = (\mathcal{B}\mathbf{u}|_\Gamma)_{-n}(z) + (\mathcal{T}L\mathbf{v})_{-n}(z),\ z \in \Omega, \tag{75}$$

where $\mathcal{B}$ is the Bukhgeim-Cauchy operator in (68), and $\mathcal{T}$ is an operator defined component-wise for $n \geqslant 0$ by

$$(\mathcal{T}\mathbf{v})_{-n}(z) := -\frac{1}{\pi}\sum_{j=0}^{\infty}\int_\Omega v_{-n-2j}(\zeta)\frac{1}{\zeta - z}\left(\frac{\overline{\zeta}-\overline{z}}{\zeta - z}\right)^j d\xi d\eta, \quad \zeta = \xi + i\eta, \quad z \in \Omega. \tag{76}$$

□

REFERENCES

[1] E. V. Arbuzov, A. L. Bukhgeim and S. G. Kazantsev, *Two-dimensional tomography problems and the theory of A-analytic functions*, Siberian Adv. Math., **8** (1998), 1–20.

[2] H. Braun and A. Hauk, *Tomographic reconstruction of vector fields*, IEEE Transactions on signal processing **39** (1991), 464–471.

[3] A. L. Bukhgeim, *Inversion Formulas in Inverse Problems*, chapter in Linear Operators and Ill-Posed Problems by M. M. Lavrentiev and L. Ya. Savalev, Plenum, New York, 1995.

[4] E. Derevtsov and I. Svetov, *Tomography of tensor fields in the plane*, Eurasian J. Math. Comput. Appl., **3(2)** (2015), 24–68.

[5] D. V. Finch, *The attenuated x-ray transform: recent developments*, in Inside out: inverse problems and applications, Math. Sci. Res. Inst. Publ., **47**, Cambridge Univ. Press, Cambridge, 2003, 47–66.

[6] H. Fujiwara, K. Sadiq and A. Tamasan, *A Fourier approach to the inverse source problem in an absorbing and anisotropic scattering medium*, Inverse Problems **36(1)**:015005 (2019).

[7] H. Fujiwara, K. Sadiq and A. Tamasan, *A two dimensional source reconstruction method in radiative transport using boundary data measured on an arc*, Inverse Problems **37(11)** (2021), 19pp.

[8] S. Holman and P. Stefanov, *The weighted Doppler transform*, Inverse Probl. Imaging, **4** (2010), 111–130.

[9] S. G. Kazantsev and A. A. Bukhgeim, *Inversion of the scalar and vector attenuated X-ray transforms in a unit disc*, J. Inverse Ill-Posed Probl., **15** (2007), 735–765.

[10] V. P. Krishnan, R. Manna, S. K. Sahoo, and V. A. Sharafutdinov, *Momentum ray transforms*, Inverse Problems Imaging **3 (13)** (2019), 679–701.

[11] V. P. Krishnan, R. Mishra and F. Monard *On solenoidal-injective and injective ray transforms of tensor fields on surfaces*, J. Inverse Ill-Posed Problems **27 (4)** (2019), 527–538.

[12] L. Kunyansky, E. McDugald, and B. Shearer, *Weighted Radon transforms of vector fields, with applications to magnetoacoustoelectric tomography*, Inverse Problems **39 (6)** (2023), 065014.

[13] R. K. Mishra, *Full reconstruction of a vector field from restricted Doppler and first integral moment transforms in* $\mathbb{R}^n$, J. Inverse Ill-Posed Problems **28** (2019), 173–184.

[14] S. J. Norton, *Tomographic reconstruction of 2-D vector fields: application to flow imaging*, Geophysical Journal **97 (1)** (1989), 161–168.

[15] D. Omogbhe and K. Sadiq, *An inverse source problem for linearly anisotropic radiative sources in absorbing and scattering medium*, Applicable Analysis, (2023), doi:10.1080/00036811.2023.2234387.

[16] V. Palamodov, *Reconstruction of a differential form from doppler transform*, SIAM Journal on Mathematical Analysis, **41(4)** (2009), 1713–1720.

[17] G. P. Paternain, M. Salo, and G. Uhlmann, *Tensor Tomography: Progress and Challenges*, Chin. Ann. Math. Ser. B., **35(3)** (2014), 399–428.

[18] K. Sadiq and A. Tamasan, *On the range of the attenuated Radon transform in strictly convex sets*, Trans. Amer. Math. Soc., **367(8)** (2015), 5375–5398.

[19] K. Sadiq and A. Tamasan, *On the range characterization of the two dimensional attenuated Doppler transform*, SIAM J. Math. Anal., **47(3)** (2015), 2001–2021.

[20] K. Sadiq, A. Tamasan, *On the range of the X-ray transform of symmetric tensors compactly supported in the plane*, Inverse Probl. Imaging **17(3)** (2023), 660–685.

[21] K. Sadiq, O. Scherzer, and A. Tamasan, *On the X-ray transform of planar symmetric 2-tensors*, J. Math. Anal. Appl., **442(1)** (2016), 31–49.

[22] T. Schuster, *20 years of imaging in vector field tomography: a review*. In Y. Censor, M. Jiang, A.K. Louis (Eds.), *Mathematical Methods in Biomedical Imaging and Intensity-Modulated Radiation Therapy (IMRT)*, in: Publications of the Scuola Normale Superiore, CRM **7** (2008) 389–424.

[23] V. A. Sharafutdinov, *Integral geometry of tensor fields*, VSP, Utrecht, 1994.

[24] G. Sparr, K. Stråhlén, K. Lindström, and H. W. Persson, *Doppler tomography for vector fields,* Inverse Problems, **11** (1995), 1051–1061.

[25] A. Tamasan, *An inverse 2D boundary value problem in radiation transport*, Ph.D. thesis, University of Washington, 2002.

[26] A. Tamasan, *Tomographic reconstruction of vector fields in variable background media*, Inverse Problems **23** (2007), 2197–2205.

[27] N. L. Thompson and A. L. Bukhgeim, *Scalar and vector tomography for the weighted transport equation with application to helioseismology*, J. Inverse Ill-Posed Probl., **31(1)** (2023), 117–145.
[28] I. N. Vekua, *Generalized Analytic Functions*, Pergamon Press Ltd. 1962.
[29] P. T. Wells, M. Halliwell, R. Skidmore, A. J. Webb, and J. P. Woodcock, *Tumour detection by ultrasonic Doppler blood-flow signals*, Ultrasonics **15(5)** (1977), 231–232.

GRADUATE SCHOOL OF INFORMATICS, KYOTO UNIVERSITY, YOSHIDA HONMACHI, SAKYO-KU, KYOTO 606-8501, JAPAN
Email address: fujiwara@acs.i.kyoto-u.ac.jp

FACULTY OF MATHEMATICS, COMPUTATIONAL SCIENCE CENTER, UNIVERSITY OF VIENNA, OSKAR-MORGENSTERN-PLATZ 1, 1090 VIENNA, AUSTRIA
Email address: david.omogbhe@univie.ac.at

JOHANN RADON INSTITUTE FOR COMPUTATIONAL AND APPLIED MATHEMATICS (RICAM), ALTENBERGERSTRASSE 69, 4040 LINZ, AUSTRIA
Email address: kamran.sadiq@ricam.oeaw.ac.at

DEPARTMENT OF MATHEMATICS, UNIVERSITY OF CENTRAL FLORIDA, ORLANDO, 32816 FLORIDA, USA
Email address: tamasan@math.ucf.edu